Search for Electronic Phase Separation at Quantum Phase Transitions

C. Pfleiderer · P. Böni · C. Franz · T. Keller · A. Neubauer · P.G. Niklowitz · P. Schmakat · M. Schulz · Y.-K. Huang · J.A. Mydosh · M. Vojta · W. Duncan · F.M. Grosche · M. Brando · M. Deppe · C. Geibel · F. Steglich · A. Krimmel · A. Loidl

Abstract Phase separation and extreme sensitivity to disorder and defects are key features of electronic order near quantum phase transitions. Neutron depolarization

C. Pfleiderer (✉) · P. Böni · C. Franz · A. Neubauer · P.G. Niklowitz · P. Schmakat · M. Schulz
Physik Department E21, Technische Universität München, 85748 Garching, Germany
e-mail: Christian.Pfleiderer@frm2.tum.de

T. Keller · M. Schulz
Forschungsneutronenquelle Heinz Maier-Leibniz (FRM II), Technische Universität München, 85748 Garching, Germany

P.G. Niklowitz · W. Duncan · F.M. Grosche
Department of Physics, Royal Holloway, University of London, Egham TW20 0EX, UK

T. Keller
Max-Planck-Institut für Festkörperforschung, 70569 Stuttgart, Germany

Y.-K. Huang
Van der Waals-Zeeman Institute, University of Amsterdam, 1018XE Amsterdam, The Netherlands

J.A. Mydosh
Kamerlingh Onnes Laboratory, Leiden University, 2300RA Leiden, The Netherlands

M. Brando · M. Deppe · C. Geibel · F. Steglich
Max-Planck-Institut für Chemische Physik fester Stoffe, 01187 Dresden, Germany

A. Krimmel · A. Loidl
Experimentalphysik V, Elektronische Korrelationen und Magnetismus, Institut für Physik, Universität Augsburg, 86135 Augsburg, Germany

F.M. Grosche
Cavendish Laboratory, University of Cambridge, Cambridge, UK

M. Vojta
Institute for Theoretical Physics, Universität zu Köln, 50937 Köln, Germany

imaging and neutron Larmor diffraction are new experimental techniques capable of providing detailed real-space and reciprocal-space information, respectively, on the existence and nature of phase separations. Proof-of-principle depolarization imaging in $Pd_{1-x}Ni_x$, $CePd_{1-x}Rh_x$ and $NbFe_2$ suggests distinct differences of the real-space distribution of ferromagnetic moments and Curie temperatures in materials at ferromagnetic quantum phase transitions. This compares with neutron Larmor diffraction which provides high-resolution reciprocal-space information of phase separation and the absence of quantum criticality in the itinerant helimagnet MnSi or the parasitic nature of small moment antiferromagnetism in URu_2Si_2.

1 Introduction

Quantum phase transitions attract great interest as the possible origin of novel forms of electronic order. The most prominent examples of such phases may be the emergence of superconductivity, density waves or partial order at the border of magnetism [15, 27, 40, 41]. However, in contrast to conventional phase transitions, which are driven by thermal fluctuations and a reduction of entropy, quantum phase transitions are generally driven by quantum fluctuations in the presence of strong competing interactions. By design quantum phase transitions are therefore sensitive to weak interactions and the 'novel' behavior found near quantum phase transitions frequently concerns the nature and origin of electronic phase coexistence of conventional forms of order. In turn microscopic evidence of electronic phase separations is of great interest in a large number of materials.

For many years neutron scattering has provided the perhaps most powerful microscopic probe of ordering phenomena in condensed matter systems. In this review we advertise two powerful techniques based on the use of polarized neutrons, notably depolarization imaging and Larmor diffraction, which became available for real experiments only recently. Both techniques are highly complementary and have their own potential when searching for possible electronic phase separations at quantum phase transitions.

Our paper is organized as follows. In the first part we describe how the depolarization of a neutron beam may be used to image ferromagnetic phase separation in real space. In proof-of-principle studies we have applied this technique to several materials in the vicinity of a ferromagnetic quantum phase transition. In the following we present first results of that part of our work which concerns different aspects of compositional tuning of ferromagnetic quantum criticality. In $Pd_{1-x}Ni_x$ ferromagnetism is stabilized when Ni is added. This compares with substitutional doping in $CePd_{1-x}Rh_x$ and changes of composition in $Nb_{1-y}Fe_{2-y}$. Our results thereby establish the power of depolarization imaging to identify inhomogeneities that originate in metallurgical complexities. This provides important insights how to improve the conditions for studies of fragile new forms of order.

The second part of our review is concerned with Larmor diffraction as a new technique for reciprocal space imaging of phase separation at quantum phase transitions. The basic information thereby consists in very high-resolution data of the lattice spac-

ing as well as the distribution of lattice constants. Being particularly suited for studies of non-ferromagnetic materials, e.g., antiferromagnetic quantum phase transitions, we review proof-of-principle studies of the itinerant helimagnet MnSi and the heavy-fermion superconductor URu_2Si_2.

2 Neutron Depolarization Imaging

2.1 Experimental Technique

The perhaps oldest imaging method based on neutrons exploits differences of the transmission of a neutron beam through a given sample due to element-specific absorption. This technique corresponds essentially to a photographic pin-hole camera. In a conventional set-up the resolution may be as low as several hundreds μm depending on the collimation of the neutron beam and the spatial resolution of a detector placed behind the sample. In recent years, proof-of-principle studies have demonstrated the possibility to improve the resolution down to several tens μm by means of dark-field imaging [9, 10]. In addition tomographic neutron imaging techniques have been developed that provide three-dimensional images. Even time-dependent processes may be recorded by means of stroboscopic methods.

The neutron imaging described so far is based on strong nuclear interactions. A second route to real-space imaging using neutrons may be based on the spin of the neutron, which undergoes Larmor precession in a magnetic field. This changes the polarization direction of particular trajectories in the beam. The depolarization of the integrated neutron beam may hence serve as a probe of the magnetic field distribution of a sample. As for the conventional neutron imaging described above neutron depolarization of the integrated beam has also been known for a long time. Recently, however, spatially resolved depolarization imaging has been developed as a tool to map out magnetic fields. Proof-of-principle studies have been reported for solenoids and materials with fairly uniform internal fields, such as superconducting materials (these studies exploited mostly a rotation of the spin polarization instead of a genuine depolarization) [12].

As a probe of magnetic field distributions depolarization imaging provides an ideal experimental tool to address the wide range of challenges posed by ferromagnetic materials. For instance, ferromagnetic domains are one of the most important aspects relevant for technical applications. A wide variety of techniques have been developed to study magnetic domains, ranging from classical Bitter decoration over magneto-optical Kerr microscopy to spin sensitive scanning microscopy. However, these techniques provide only information on magnetic domains at surfaces and in thin films, while the nature of magnetic domains in bulk samples is still an open issue. Another example concerns the possible coexistence of ferromagnetism with other forms of order, notably superconductivity or density waves. These types of coexistence occur in rather complex oxide materials, such as the rutheno-cuprates or certain GMR materials. They are also a major topic of interest in studies of quantum phase transitions of intermetallic compounds.

Motivated by the wide range of open scientific questions we have started to adapt the depolarization imaging technique for studies of ferromagnetic quantum phase

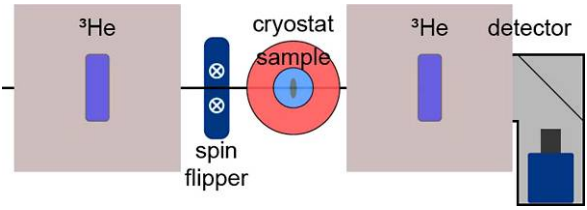

Fig. 1 (Color online) Typical neutron depolarization imaging set up used in the studies described in this article. A ^{3}He polarizer and analyzer were used. A spin-flipper is located between polarizer and sample cryostat. The detector is placed directly behind the analyzer for increased resolution, where the CCD camera to read out the scintillator image plate is separated by a mirror to reduce the parasitic background signal

transitions. This required systematic tests how to improve the spatial resolution, the implementation of the depolarization technique down to milli-Kelvin sample temperatures and advances in the interpretation of the measured signals (see e.g. [38]).

In a first effort we addressed the question, how to achieve simultaneously high spatial resolution and high intensity. Conceptually the set up used in depolarization imaging consists of a polarizer before the sample, followed by an analyzer and an image detector. We have tested various combinations of polarizers and analyzers as described, e.g., in Ref. [38]. For most applications the most powerful set up turned out to be polarizing ^{3}He cells and the use of a polychromatic beam (see also Fig. 1). These provide a high degree of polarization and the polarization is uniform across the neutron beam without optical artifacts.

To explore the potential of depolarization imaging we have studied $Pd_{1-x}Ni_x$, $CePd_{1-x}Rh_x$ and $Nb_{1-y}Fe_{2-y}$ as well as Fe_2TiSn, Fe_2VAl and Ni_3Al. In the following we review first results obtained in the first three compounds. These results illustrate the insights that may be obtained through depolarization imaging and the feasibility of developments that may become possible in the future.

2.2 $Pd_{1-x}Ni_x$

The exchange enhanced paramagnet Pd stabilizes ferromagnetic order when a small amount of Ni is added. Detailed studies of polycrystalline sample suggested the existence of a ferromagnetic quantum critical point at $x_c \approx 2.5\,\%$. As x_c is approached the canonical properties predicted for an itinerant electron ferromagnet are observed [21], i.e., a logarithmic divergence of the specific heat $C/T \propto \ln T$, a temperature dependence of the resistivity $\Delta\rho \propto T^{5/3}$ and the usual mean-field divergence of the susceptibility $\chi^{-1} \propto T^{4/3}$. However, these properties are expected in pure compounds while $Pd_{1-x}Ni_x$ clearly contains disorder. We therefore decided to revisit the properties of $Pd_{1-x}Ni_x$ by means of neutron depolarization.

We began our studies on four Czochralsky grown samples of different compositions near x_c purchased from Mateck. One of the samples was single crystalline, but the properties were rather similar for all four of them. The magnetic field dependence of the magnetization of theses samples, which was previously not studied in detail, was consistent with a ferromagnetic quantum critical point [8]. However, for

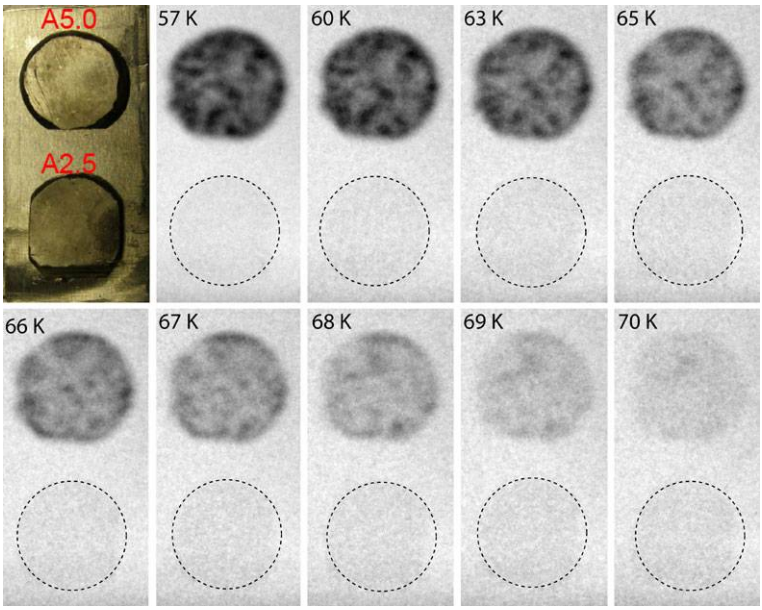

Fig. 2 (Color online) Typical neutron depolarization images of two polycrystalline $Pd_{1-x}Ni_x$ discs at various temperatures. For increasing depolarization the gray-scale become darker and is essentially black for complete depolarization. Note the variations across the upper disc at fixed intermediate temperatures. Bulk properties of samples from the same growth are reported in Ref. [21]. The Ni concentrations of the discs at the top and bottom are 5% and 2.5%, respectively. The photograph at the top left corner shows the samples as mounted for the measurements in an Al frame. Small variations of the depolarization and Curie temperature are observed across the 5% sample, while the 2.5% sample is non-magnetic down to 4 K, the lowest temperature measured

low magnetic fields we found systematic deviations of the magnetization from mean-field behavior. First depolarization imaging studies revealed large variations of the distribution of Curie temperatures for all compositions. For preliminary results on a tomographic reconstruction we refer to Ref. [37].

In addition two polycrystalline samples with Ni contents of $x = 2{:}50\%$ (A2.5) and $x = 5{:}00\%$ (A5.0), respectively, made at the University of Augsburg, were investigated. These samples had a diameter of 10 mm and a thickness of 2 mm. They were prepared by arc melting in argon and quenched from the melt and annealed at 1000 °C for five days, following the same procedure employed for the samples studied in Ref. [21]. The depolarization studies were carried out with the set up described above and a monochromatic neutron beam with $\lambda = 3.2$ Å. Data were recorded down to 4 K, the lowest temperature available.

While sample A5.0 showed strong depolarization of the beam, no depolarization was found for sample A2.5 down to 0.4 K, the lowest temperature measured, consistent with [21]. To better determine the Curie temperature and homogeneity of sample A5.0, a temperature scan of the neutron depolarization from 55 K to 75 K was made in steps of 1 K (Fig. 2). The resulting T_C (not shown) is rather homogeneous compared to those found in the crystal purchased from Mateck. However, there are still variations of T_C between 66 K to 73 K in general agreement with [21]. Taken together the

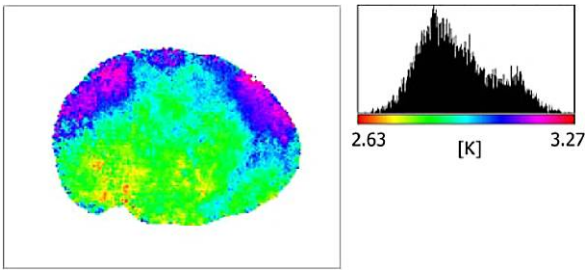

Fig. 3 (Color online) Typical data of a disc of single-crystal $CePd_{1-x}Rh_x$ ($x = 0.6$) (from left to right the largest distance is roughly 10 mm). The sample was cut straight from the ingot as grown. The well defined gradient in the colour distribution suggests a composition gradient from bottom to top of the ingot induced by directional freezing. A fairly narrow distribution of Curie temperatures of order 10% is observed as shown in the *inset*. The known $T_c(x)$ dependence implies variations of the composition of a few tenths of a percent

polycrystalline samples are much more homogeneous than the Czochralsky grown crystals as expected from the metallurgical phase diagram.

2.3 $CePd_{1-x}Rh_x$

The binary compound CePd is one of the few Ce-based ferromagnets, where the Curie temperature is $T_C = 6.5$ K. Substitutional replacement of Pd by Rh causes a suppression of the ferromagnetism, which vanishes above a critical concentration $x_c \approx 0.85$. In recent years detailed studies of polycrystals and single-crystals of $CePd_{1-x}Rh_x$ have provided evidence of the formation of a new type of electronic ground state—the Kondo cluster glass [39, 44]. This state may be visualized as the formation of clusters of Kondo-screened moments an a nm scale, that freeze collectively below a characteristic temperature.

Even though the length scale characterizing the Kondo cluster glass is only of the order of several nm, which is well below the resolution limit offered by any real-space imaging technique based on neutrons, we decided to perform a first series of feasibility tests to explore this state further. For our studies a bespoke cryogen free ^{3}He system was set up for use with the depolarization set up. The depolarization set up was unchanged as described above. The polycrystals and single crystals studied were the same prepared for the study reported in the Ref. [44].

Shown in Fig. 3 is a real space map of the Curie temperatures inferred from the onset of the depolarization as a function of temperature. Note that the sample characterized here represents a cross-section of the entire ingot as grown. Its is interesting to note that the sample shows a small gradient of the Curie temperatures from top to bottom. As the sample was resting on a water-cooled copper hearth (at the bottom side) this suggests that the precise composition is also related to the direction of cooling. This may ultimately provide important information how to improve the sample quality. The inset of Fig. 3 displays the probability distribution at which different Curie temperatures occur across the section studied, where the data were analyzed on a square grid with 0.5 mm spacing (slightly larger then the resolution limit).

While the Curie temperatures range from about 2.8 K to about 3.1 K, the distribution is narrow ($\sim$10 %) as compared to the distribution of Curie temperatures

observed in the single crystals of $Pd_{1-x}Ni_x$. In fact, using the published $T_c(x)$ dependence of $CePd_{1-x}Rh_x$ the variations of Curie temperatures correspond to variations in composition not larger than a few tenths of a percent. Thus, concerning their composition our study already establishes, that the samples are certainly much more homogeneous than the Czochralsky grown single and polycrystals of $Pd_{1-x}Ni_x$. Yet, an important question that has to be left for future studies concerns the extent to which the cluster glass is driven microscopically by the precise distribution of the atoms. Moreover, we have not been able yet to study the depolarization at the lowest temperatures in the cluster glass state.

2.4 $Nb_{1-y}Fe_{2-y}$

The third example of a system in which composition controls the distance to ferromagnetic quantum criticality may be found in the hexagonal C14 Laves phase compound $Nb_{1-y}Fe_{2-y}$. For $y \to 0.012$ ferromagnetism decreases. In other words, both Nb-rich and Nb-poor samples are ferromagnetic. In this compound a relative shift of composition is exploited, rather than addition of a different element or substitutional doping as in $CePd_{1-x}Rh_x$.

The bulk properties of polycrystalline samples of $Nb_{1-y}Fe_{2-y}$ and a few small single crystals display marginal Fermi liquid behavior for slightly Fe poor $NbFe_2$, when T_C has vanished, characteristic of a ferromagnetic quantum critical point [5, 18]. For slightly Fe-rich samples the ferromagnetic transition is preceded as a function of temperature by the signatures of a putative density wave instability. As the density wave instability seems intimately connected with the vicinity to ferromagnetic quantum criticality it has been suggested that it is driven by strong electronic correlations rather than single-particle nesting. This may be expected in recent scenarios of a break-down of the Ginzburg-Landau-Wilson theory of itinerant-electron ferromagnetic quantum criticality.

To explore the nature of ferromagnetic quantum criticality and the density wave instability in $Nb_{1-y}Fe_{2-y}$ we have grown several large single crystals by means of optical float zoning in a UHV-compatible image furnace at Munich [7]. The polycrystalline starting rods were prepared from high-purity starting elements at Royal Holloway, London. The published binary phase diagram of $Nb_{1-y}Fe_{2-y}$ thereby shows a wide homogeneity range. In a first characterization using x-rays and single-crystal neutron diffraction as well as the canonical bulk properties (magnetization, susceptibility and specific heat) we find very sharp phase transitions and all the characteristics expected of high quality single crystals.

Shown in Fig. 4 are typical data observed in depolarization imaging of one of the single crystals grown for our studies. For the depolarization study two adjacent parts of the ingot were placed next to each other on an Al support as shown in the photograph. As a function of temperature we observe very homogeneous magnetic properties. However, there are essentially two distinct sections of the ingot one of which shows ferromagnetism and a sharp Curie temperature, while the other section does not develop ferromagnetism down to 4 K. In fact, we have confirmed that this section does not become ferromagnetic even down to 0.4 K.

The excellent homogeneity of depolarization and the very sharp Curie temperature, when taking into account the temperature versus composition phase diagram,

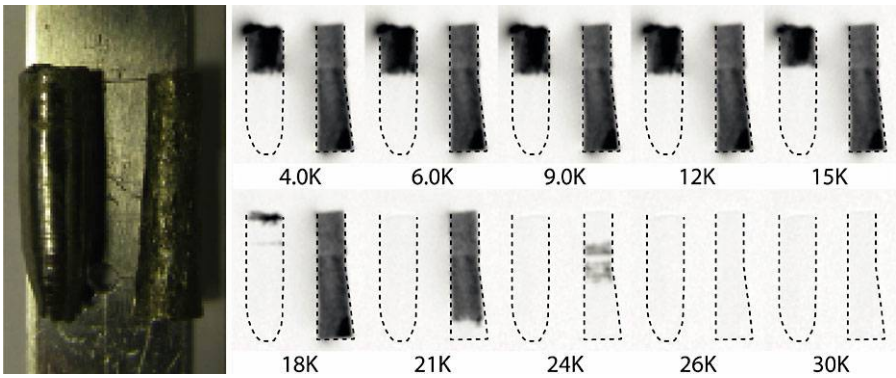

Fig. 4 (Color online) Typical depolarization imaging of a single crystal of $Nb_{1-y}Fe_{2-y}$ grown by optical float zoning. Two adjacent parts of the ingot were placed next to each other and studied simultaneously. The bottom end of the segment on the left hand side did not show any signs of ferromagnetism down to 0.4 K, the lowest temperature studied

implies an excellent sample quality. This identifies $Nb_{1-y}Fe_{2-y}$ as an ideal system for studies of the interplay of ferromagnetism and quantum criticality. However, since the polycrystalline starting material was carefully prepared to be ideally homogeneous throughout we have no explanation for the sudden change of the ferromagnetic properties during the single-crystal growth. This motivates detailed studies of the metallurgy of $Nb_{1-y}Fe_{2-y}$ planned for the future.

3 Neutron Larmor Diffraction

3.1 Experimental Technique

We now turn to a fairly new neutron scattering method, Larmor diffraction, that allows to obtain reciprocal space information on the presence and nature of electronic phase separation. Larmor diffraction permits high-intensity measurements of lattice constants with an unprecedented high resolution of $\Delta a/a \approx 10^{-6}$ [13, 14, 35]. Of course this resolution is far inferior to the resolution available in standard capacitive dilatometry ($\Delta a/a \approx 10^{-10}$), yet it is sufficient for high pressure studies, where standard techniques may not be applied. The first proof-of-principle studies using this technique were performed at the triple-axis spectrometer FLEX at Berlin [13, 35]. Our LD measurements were carried out at the spectrometer TRISP at FRM II (Munich). As shown in Fig. 5 in LD the sample is illuminated by a polarized neutron beam (arrows indicate the polarization). The neutron resonance spin flipper coils, denoted as C1 through C4 in Fig. 5, serve to encode the scattering angle in the polarization direction.

The coils C1 through C4 thereby continuously change the polarization direction of the beam as a function of time. The coils C1 and C3 are set up such, that they generate a time dependence of the polarization as if the polarization would precess in the scattering plane at twice the radio frequency ω of the coils. The coils C2 and C4

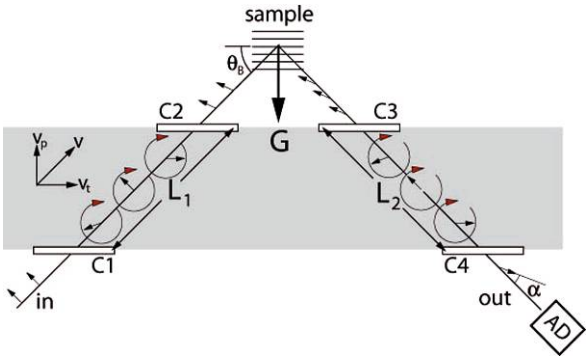

Fig. 5 (Color online) Schematic depiction of the principle of Larmor diffraction. The neutron resonance spin flipper coils C1 through C4 generate a time dependence of the polarization orientation of the neutron beam in the gray shaded area. The time dependence may be viewed as a Larmor precession that encodes the scattering angle (and hence lattice spacing) in the total phase of precession as explained in the text

are tuned to terminate this time-dependence of the polarization; at any given location in the gray shaded regime the beam polarization hence appears to precess even though there is no applied magnetic field.

The coils C1 through C4 are aligned *parallel* to the lattice planes, because this way changes of the lattice spacing a sensitively affect the total time of travel t_{tot} along $L = L_1 + L_2$ (t_{tot} is purely determined by the velocity component v_p of the neutrons parallel to **G**). Hence, the total phase of precession Φ along L_1 plus L_2 depends linearly on the lattice constant a: $\Phi = 2\omega Lma/(\pi\hbar)$ (m is the mass of the neutron [14, 28, 35]). Changes of a affect the angle α and thus the intensity recorded by the polarization analyzer and detector 'AD'. In turn change of total phase are determined most efficiently by recording the intensity as a function of the position of C4, which may be moved very accurately along the beam direction. These data provide not just information on the lattice constant. When recording the polarization of the neutron beam as a function of Larmor frequency the distribution of lattice constants across the entire sample volume may be measured, which is not accessible with any other technique.

3.2 MnSi

The temperature versus pressure phase diagram of the itinerant-electron magnet MnSi suggests the emergence of a genuine non-Fermi liquid state at high pressure, separated by a first order transition and phase segregation from conventional order at low pressure (Fig. 6(a)) [30, 31]. At ambient pressure MnSi develops helimagnetic order below $T_c = 29.5$ K in a well-understood Fermi liquid ground state. Under hydrostatic pressure the transition temperature as measured in the resistivity and AC susceptibility decreases and vanishes above $p_c = 14.6$ kbar. In high purity single crystals the transition, as measured in the AC susceptibility, changes from first to second order for pressures exceeding $p^* \approx 12$ kbar. This is accompanied by itinerant-electron metam-

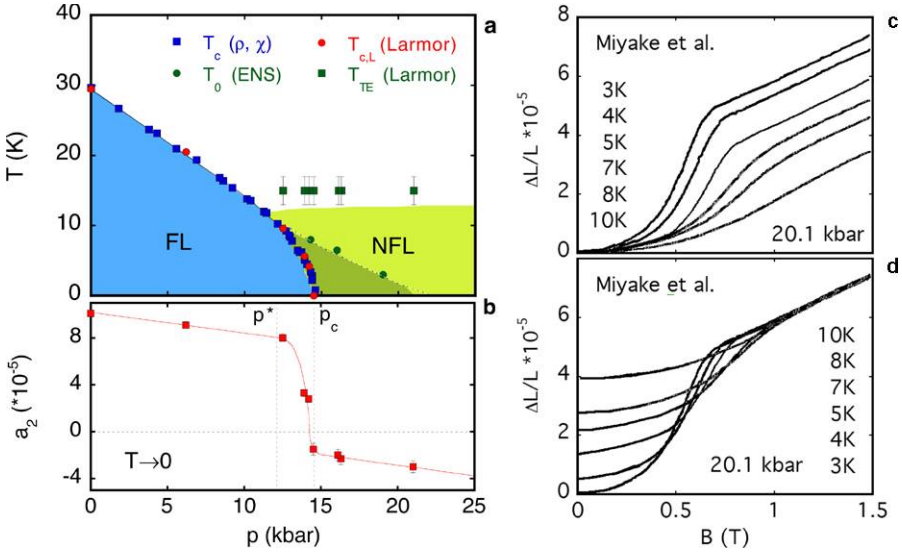

Fig. 6 (Color online) (**a**) Temperature versus pressure phase diagram of MnSi as reported in Ref. [28]. (**b**) Extrapolated zero temperature magnetic contribution to the lattice constant. Between $p^* \approx 12$ kbar and $p_c \approx 14.6$ kbar this signal decreases in agreement with the reduction of the volume fraction of helical order seen in independent neutron scattering and μ-SR studies, characteristic of phase separation. Note the negative contribution above p_c. (**c**) Published forced magnetostriction in MnSi at high pressure as measured with strain gauges. Data were taken from Ref. [17]. Curves correspond from top to bottom to the temperatures given on the right hand side. (**d**) Same data as shown in (**d**), but now plotted such that data at high fields correspond. Curves correspond from top to bottom to the temperatures given on the left hand side. This brings out the emergence of the negative contribution at low fields and low temperatures, which corresponds quantitatively to the negative value shown in (**b**)

agnetism under magnetic fields [42], which strongly underscores the first order nature of the transition in the range $p^* < p < p_c$[1].

As the most remarkable property the low temperature electrical resistivity of MnSi changes with increasing pressure from the quadratic dependence of an enhanced Fermi liquid to a $T^{3/2}$ non-Fermi liquid dependence above p_c [30]. The extended temperature versus pressure regime in which this $T^{3/2}$ resistivity is observed, suggested early on that it is not related to quantum criticality. This is corroborated by evidence of a decreasing volume fraction of helical ordering in samples of differing quality in the range $p^* < p < p_c$. For instance, elastic neutron scattering as a function of temperature and pressure established partial magnetic order above p_c [34]. Its signatures already appear in the range $p^* < p < p_c$, where the temperature dependence is distinctly different from the helical order. This is strongly supported by the magnetic field dependence observed in small angle neutron scattering [33]. In

[1]Recent susceptibility studies in zero applied field [26] claim a first order transition for $p \ll p^*$. These measurements have not been backed up by the magnetic field dependence. Similar data were observed in our studies which could be attributed to domain populations, i.e., the features are not intrinsic to the itinerant-electron state.

addition, muon-spin-rotation studies [43] establish the same reduction of the volume fraction of helimagnetic order in the range $p^* < p < p_c$.

The most direct evidence that the non-Fermi liquid resistivity emerges without quantum criticality has been observed by means of Lamor diffraction [28]. The same data also clearly show the formation of phase separation in the range $p^* < p < p_c$. The magneto-elastic contribution as extrapolated to zero temperature thereby tracks the helimagnetic volume fraction inferred from the μSR study [43][2]. The absence of quantum criticality is inferred from the change from magneto-expansion to magnetostriction at p_c (Fig. 6(b)), which exists below $T^* = 12$ K (for a QCP $T^* = 0$). The Larmor data thereby show that the regime of the non-Fermi liquid resistivity is accompanied by a magnetostriction at 20 kbar of roughly $a_2 \approx 4 \times 10^{-5}$. The same magnetostriction may also be inferred from forced magnetostriction measurements reported by Miyake et al. [17]. This may be seen by normalizing the original data (shown in Fig. 6(c)) at high magnetic fields as shown in Fig. 6(d).

3.3 URu_2Si_2

We have also used Larmor diffraction to resolve the nature of the temperature versus pressure phase diagram of the heavy fermion superconductor URu_2Si_2 [22]. The long-standing puzzle in URu_2Si_2 concerns the observation of an unknown form of electronic order (known as hidden order) at ambient pressure below $T_0 = 17.5$ K [16, 24, 25, 36], which turns into large moment Ising antiferromagnetism for hydrostatic pressures exceeding ~ 5 kbar [3]. The discovery of Ising antiferromagnetic order with tiny moments in the regime of the hidden order [6] has inspired a wide range of experimental and theoretical studies concerning the possible relationship of the large-moment antiferromagnetism, small-moment antiferromagnetism and the hidden order.

In our studies we have measured the temperature and pressure dependence of the lattice constants of a high purity single crystal of URu_2Si_2 with Larmor diffraction. The ordered magnetic moment was monitored with the same setup using conventional diffraction. For our studies a Cu:Be clamp cell was used with a Fluorinert mixture [29] and the pressure was inferred at low temperatures from the (002) reflection of graphite as well as absolute changes of the lattice constants of URu_2Si_2. The single crystal studied was grown by means of an optical floating-zone technique at the Amsterdam/Leiden Center. High sample quality was confirmed via X-ray diffraction and detailed electron probe microanalysis. Samples cut-off from the ingot showed good resistance ratios (20 for the c axis and ≈ 10 for the a axis) and a high superconducting transition temperature $T_c \approx 1.5$ K. The magnetization of the large single crystal agreed very well with data shown in Ref. [32] and confirmed the absence of

[2]Recent μ-SR measurements purport to find no evidence for phase separation [4] based on misleading claims of good experimental conditions. In contrast to what is stated in this paper the sample quality as measured by the residual resistivity ratio of 40 is worse than in any of our studies (in our samples the RRRs range between 100 and 500). Moreover, the pressure conditions are at best identical to our studies (we used a variety of different pressure transmitters including those used in Ref. [4]). A simple explanation for the absence of phase separation seen in [4] is a suppression of the phase separation due to pinning and defects for the low sample quality studied.

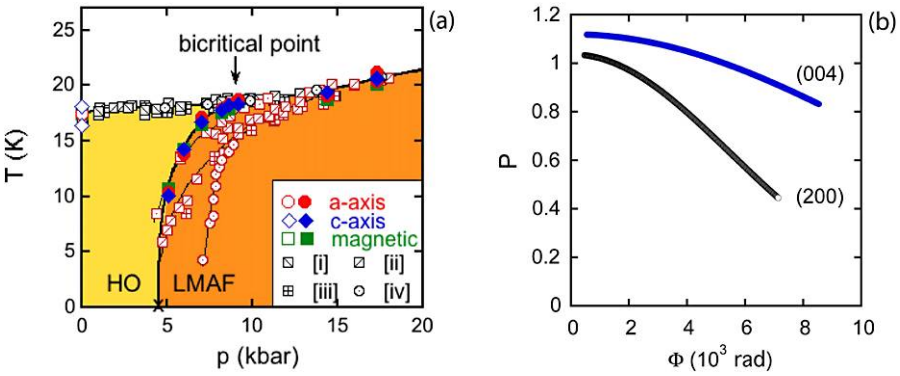

Fig. 7 (Color online) (**a**) Temperature versus pressure phase diagram of URu_2Si_2 and comparison with previous published work (the symbols are taken from the following references (i): Ref. [19], (ii): Ref. [11], (iii): Ref. [20], (iv): Ref. [2]). The HO and LMAF are separated by a line of first order transitions ending in a bicritical point. This implies that HO and LMAF have different symmetry and must be coupled non-linearly. (**b**) Change of the polarization of the neutron beam as a function of total Larmor phase. The decrease reflects the distribution of lattice constants. From the measured distribution of lattice constants the distribution of ratios of lattice constants $\Delta\eta/\eta$ may be inferred. In turn, the volume fraction for which the ratio of lattice constants exceeds the threshold to LMAF determined in uniaxial stress studies, explains the observed SMAF in the HO at ambient pressure [22, 23]

ferromagnetic inclusions. Most importantly, in our neutron scattering measurements we found an antiferromagnetic moment $m_s \approx 0.012\mu_B$ per U atom, which matches the smallest moment reported so far [2].

Measurements of the depolarization of the neutron beam as a function of Larmor frequency were used to determine the distribution of lattice constants of the a- and c-axis, respectively (Fig. 7(b) shows the depolarization as a function of the associated total Larmor phase). Assuming a Gaussian distribution of both lattice constants, we find a full width at half-maximum of the distribution of the ratio of lattice constants $f(\Delta\eta/\eta)_{\mathrm{FWHM}} \approx 6.4 \times 10^{-4}$. Based on neutron scattering studies of the effect of uniaxial stress on the antiferromagnetic signal it has been suggested [45], that antiferromagnetism stabilizes when the ratio of lattice constants exceeds a threshold $\Delta\eta_c/\eta \approx 5 \times 10^{-4}$. Thus, for the measured distribution of ratios of lattice constants the volume fraction with LMAF corresponds to an average magnetic moment of $0.013(5)\mu_{\mathrm{B}}$. This is in excellent quantitative agreement with the experimental value and identifies the SMAF as being purely parasitic.

In addition we have measured the lattice constants and magnetic moments as a function of pressure under the exact same conditions. This allowed us to track both the lattice anomaly and the antiferromagnetic moment as a function of pressure providing unambiguous evidence of a line of first order transitions separating the HO and LMAF, which ends in a bicritical point. In comparison with previous studies we find the lowest value of p_c as shown in Fig. 7 and a very fast (discontinuous) increase of the transition temperature. As a consequence the coupling between the HO and LMAF do not have the same symmetry and must be coupled non-linearly. This supports exotic scenarios of the HO such as, incommensurate orbital currents, helicity order, or multipolar order.

4 Future Challenges

Phase segregations play an increasingly important role in the discussion of quantum phase transitions. The effects observed may be either related to metallurgical complexities or intrinsic. In our first studies of ferromagnetic quantum phase transitions using depolarization imaging we already obtained important insight on the metallurgical quality of the samples studied. While insoluble systems like $Pd_{1-x}Ni_x$ show strong inhomogeneities, depolarization imaging established small concentration variations across the ingot of Bridgman grown $CePd_{1-x}Rh_x$ and a rather excellent sample homogeneity in optically float-zoned $Nb_{1-y}Fe_{2-y}$. To improve our understanding of the interplay of metallurgical properties and phase segregations it will be necessary to improve the resolution in depolarization imaging.

Two different approaches to boost the resolution are conceivable. First, neutron optics has been improved to a level that neutron beams may be focused to a spot size of a few micro-meters only. Proof-of-principle experiments on tiny NiS_2 samples have established the suitability of this technique for high pressure studies [23]. The same type of neutron optics may be combined with a high precision position stage to scan samples systematically point by point. The higher density of the focused beam will thereby compensate the time needed for scanning the sample point by point.

Second, so-called dark field imaging techniques which exploit differences of scattering density, have been used in recent years for high resolution imaging. This technique has even been applied to map out magnetic domains with a resolution of a few ten micro-meters [9, 10]. However, neutron dark field imaging so far uses non-polarized neutrons. The precise nature of the differences of scattering density, which may be due to both nuclear or dipolar interactions, remain ambiguous. An important aspect to be developed in the future is therefore combined depolarization and dark field imaging for studies of ferromagnetic textures.

Similar to the improvements of real space imaging with neutrons it is also planned to advance the resolution available in Larmor diffraction. Dynamic scattering theory thereby imposes a fundamental resolution limit $\Delta d/d \approx 10^{-7}$. This limit may be readily reached when increasing the scattering angle and the distance over which Larmor precession takes place. Using a simple back-scattering configuration a cost-effective dedicated Larmor diffractometer may be built. As for the radiographic imaging bespoke neutron optic will allow to reduce the minimum sample volume necessary for meaningful studies.

An interesting question concerns finally, whether Larmor diffraction may even be applied to ferromagnetic materials. The depolarization of the neutron beam in soft ferromagnets, exploited in depolarization imaging, is of course detrimental for Larmor diffraction. However, in a series of first experiments on the superconducting Ising ferromagnet UGe_2 we have found that the polarization remains sufficiently high for meaningful Larmor diffraction measurements [1].

Acknowledgements We gratefully acknowledge financial support in the framework of the focused research unit on Quantum Phase Transitions FOR960 of the German Science Foundation (DFG).

References

1. D. Sokolov, R. Ritz, T. Keller, C. Pfleiderer, A.D. Huxley, in Proceedings of the International Conference on Strongly Correlated Electron Systems (2010)
2. H. Amitsuka, K. Matsuda, I. Kawasaki, K. Tenya, M. Yokoyama, C. Sekine, N. Tateiwa, T.C. Kobayashi, S. Kawarazaki, H. Yoshizawa, J. Magn. Magn. Mater. **310**, 214 (2007)
3. H. Amitsuka, M. Sato, N. Metoki, M. Yokoyama, K. Kuwahara, T. Sasakibara, H. Morimoto, S. Kawarazaki, Y. Miyako, J.A. Mydosh, : Effect of pressure on tiny antiferromagnetic moment in the heavy-electron compound URu_2Si_2. Phys. Rev. Lett. **83**, 5114–5117 (1999)
4. D. Andreica, P. Dalmas de Réotier, A. Yaouanc, A. Amato, G. Lapertot, Absence of magnetic phase separation in MnSi under pressure. Phys. Rev. B **81**(6), 060412 (2010). doi10.1103/PhysRevB.81.060412
5. M. Brando, W.J. Duncan, D. Moroni-Klementowicz, C. Albrecht, D. Grüner, R. Ballou, F.M. Grosche, Logarithmic Fermi-liquid breakdown in $NbFe_2$. Phys. Rev. Lett. **101**(2), 026401 (2008)
6. C. Broholm, J.K. Kjems, W.J.L. Buyers, P. Matthews, T.T.M. Palstra, A.A. Menovsky, J.A. Mydosh, Magnetic excitations and ordering in the heavy-fermion superconductor URu_2Si_2. Phys. Rev. Lett. **58**, 1467–1470 (1987)
7. W.J. Duncan, O.P. Welzel, D. Moroni-Klementowicz, C. Albrecht, P.G. Niklowitz, D. Grüner, M. Brando, A. Neubauer, C. Pfleiderer, N. Kikugawa, A.P. Mackenzie, F.M. Grosche, Quantum phase transitions in $NbFe_2$ and $Ca_3Ru_2O_7$. Phys. Status Solidi B **247**, 599 (2010)
8. C. Franz, C. Pfleiderer, A. Neubauer, M. Schulz, B. Pedersen, P. Böni, Magnetization of $Pd_{1-x}Ni_x$ near quantum criticality. J. Phys. Conf. Ser. **200**, 012036 (2010)
9. C. Grünzweig, C. David, O. Bunk, M. Dierolf, G. Frei, G. Kühne, J. Kohlbrecher, R. Schäfer, P. Lejcek, H.M.R. Rønnow, F. Pfeiffer, Neutron decoherence imaging for visualizing bulk magnetic domain structures. Phys. Rev. Lett. **101**(2), 025504 (2008). doi10.1103/PhysRevLett.101.025504
10. C. Grünzweig, C. David, O. Bunk, M. Dierolf, G. Frei, G. Kühne, R. Schäfer, S. Pofahl, H.M.R. Rønnow, F. Pfeiffer, Bulk magnetic domain structures visualized by neutron dark-field imaging. Appl. Phys. Lett. **93**, 112504 (2008)
11. E. Hassinger, G. Knebel, K. Izawa, P. Lejay, B. Salce, J. Flouquet, Temperature-pressure phase diagram of URu_2Si_2 from resistivity measurements and ac calorimetry: Hidden order and Fermisurface nesting. Phys. Rev. B **77**, 115117 (2008)
12. N. Kardjilov, I. Manke, M. Strobl, A. Hilger, W. Treimer, M. Meissner, T. Krist, J. Banhart, Three-dimensional imaging of magnetic fields with polarized neutrons. Nat. Phys. **4**, 399 (2009)
13. T. Keller, R. Golub, F. Mezei, R. Gähler, Recent developments and results from the neutron resonance spin-echo spectrometer (NRSE) at BENSC Berlin. Physica B **234–236**, 1126–1127 (1997)
14. T. Keller, M.T. Rekveldt, K. Habicht, Neutron Larmor diffraction measurement of the lattice-spacing spread of pyrolytic graphite. Appl. Phys. A (Suppl.) **74**, 127–129 (2002)
15. H. von Löhneysen, A. Rosch, P. Wölfle, M. Vojta, Quantum phase transitions. Rev. Mod. Phys. **79**, 001015 (2007)
16. M.B. Maple, J.W. Chen, Y. Dalichaouch, T. Kohara, C. Rossel, M.S. Torikachvili, M.W. McElfresh, J.D. Thompson, Partially gapped Fermi surface in the heavy-fermion superconductor URu_2Si_2. Phys. Rev. Lett. **56**, 185–188 (1986)
17. A. Miyake, A. Villaume, Y. Haga, G. Knebel, B. Salce, G. Lapertot, J. Flouquet, Pressure collapse of the magnetic ordering in MnSi via thermal expansion. J. Phys. Soc. Jpn. **78**, 044703 (2009). arXiv:0901.4435
18. D. Moroni-Klementowicz, M. Brando, C. Albrecht, W.J. Duncan, F.M. Grosche, D. Grüner, G. Kreiner, Magnetism in Nb_{1-y} Fe_{2+y}: Composition and magnetic field dependence. Phys. Rev. B **79**(22), 224410 (2009)
19. G. Motoyama, T. Nishioka, N.K. Sato, Phase transition between hidden and antiferromagnetic order in URu_2Si_2. Phys. Rev. Lett. **90**, 166402 (2003)
20. G. Motoyama, N. Yokoyama, A. Sumiyama, Y. Oda, Electrical resistivity and thermal expansion measurements of URu_2Si_2 under pressure. J. Phys. Soc. Jpn **77**, 123710 (2008)
21. M. Nicklas, M. Brando, G. Knebel, F. Mayr, W. Trinkl, A. Loidl, Non-Fermi-liquid behavior at a ferromagnetic quantum critical point in Ni_xPd_{1-x}. Phys. Rev. Lett. **82**(21), 4268–4271 (1999)
22. P.G. Niklowitz, C. Pfleiderer, T. Keller, M. Vojta, Y.K. Huang, J.A. Mydosh, Parasitic small-moment antiferromagnetism and nonlinear coupling of hidden order and antiferromagnetism in URu_2Si_2 observed by Larmor diffraction. Phys. Rev. Lett. **104**, 106406 (2010)

23. P.G. Niklowitz, C. Pfleiderer, S. Mühlbauer, P. Böni, T. Keller, P. Link, J.A. Wilson, M. Vojta, J.A. Mydosh, New angles on the border of antiferromagnetism in NiS_2 and URu_2Si_2. Physica B **404**(19), 2955–2960 (2009). doi10.1016/j.physb.2009.07.026
24. T. Palstra, A.A. Menovsky, J. Vandenberg, A.J. Dirkmaat, P.H. Kes, G.J. Nieuwenhuys, J.A. Mydosh, Superconducting and magnetic transitions in the heavy-fermion system URu_2Si_2. Phys. Rev. Lett. **55**, 2727–2730 (1985)
25. T.T.M. Palstra, A.A. Menovsky, J.A. Mydosh, Anisotropic electrical resistivity of the magnetic heavy-fermion superconductor URu_2Si_2. Phys. Rev. B **33**, 6527 (1986)
26. A.E. Petrova, V. Krasnorussky, J. Sarrao, S.M. Stishov, Tricritical behavior in MnSi at nearly hydrostatic pressure. Phys. Rev. B **73**(5), 052409 (2006). doi10.1103/PhysRevB.73.052409
27. C. Pfleiderer, Superconducting phases of f-electron compounds. Rev. Mod. Phys. **81**(4), 1551–1624 (2009)
28. C. Pfleiderer, P. Böni, T. Keller, U.K. Rößler, A. Rosch, Non-Fermi liquid metal without quantum criticality. Science **316**, 1871 (2007)
29. C. Pfleiderer, A.D. Huxley, S.M. Hayden, On the use of Cu:Be clamp cells in magnetization and neutron scattering studies. J. Phys., Condens. Matter **17**, S3111 (2005)
30. C. Pfleiderer, S.R. Julian, G.G. Lonzarich, Non-Fermi liquid nature of the normal state of itinerant-electron ferromagnets. Nature **414**, 427–430 (2001)
31. C. Pfleiderer, G.J. McMullan, S.R. Julian, G.G. Lonzarich, Magnetic quantum phase transition in MnSi under hydrostatic pressure. Phys. Rev. B **55**, 8330 (1997)
32. C. Pfleiderer, J.A. Mydosh, M. Vojta, Pressure dependence of the magnetization of URu_2Si_2. Phys. Rev. B **74**(10), 104412 (2006). doi10.1103/PhysRevB.74.104412
33. C. Pfleiderer, D. Reznik, L. Pintschovius, J. Haug, Magnetic field and pressure dependence of small angle neutron scattering in MnSi. Phys. Rev. Lett. **99**(15), 156406 (2007)
34. C. Pfleiderer, D. Reznik, L. Pintschovius, H. v. Löhneysen, M. Garst, A. Rosch, Partial magnetic order in the non-Fermi liquid phase of MnSi. Nature **427**, 227–230 (2004)
35. M.T. Rekveldt, T. Keller, R. Golub, Larmor precession, a technique for high-sensitivity neutron diffraction. Eur. Phys. Lett. **54**, 342–346 (2001)
36. W. Schlabitz, J. Baumann, B. Pollit, U. Rauchschwalbe, H.M. Mayer, U. Ahlheim, C.D. Bredl, Superconductivity and magnetic order in a strongly interacting Fermi-system: URu_2Si_2. Z. Phys. B **62**, 171–177 (1986)
37. M. Schulz, A. Neubauer, S. Masalovich, M. Mühlbauer, E. Calzada, B. Schillinger, C. Pfleiderer, P. Böni, Towards a tomographic reconstruction of neutron depolarization data. J. Phys. Conf. Ser. **211**, 012025 (2010)
38. M. Schulz, A. Neubauer, M. Mühlbauer, E. Calzada, B. Schillinger, C. Pfleiderer, P. Böni, Polarized neutron radiography with a periscope. J. Phys. Conf. Ser. **210**, 112009 (2010)
39. J.G. Sereni, T. Westerkamp, R. Küchler, N. Caroca-Canales, P. Gegenwart, C. Geibel, Ferromagnetic quantum criticality in the alloy $CePd_{1-x}Rh_x$. Phys. Rev. B **75**(2), 024432 (2007). doi10.1103/PhysRevB.75.024432
40. G.R. Stewart, Non-Fermi-liquid behavior in d- and f-electron metals. Rev. Mod. Phys. **73**(4), 797–855 (2001). doi10.1103/RevModPhys.73.797
41. G.R. Stewart, Addendum: Non-Fermi-liquid behavior in d- and f-electron metals. Rev. Mod. Phys. **78**(3), 743–753 (2006). doi10.1103/RevModPhys.78.743
42. C. Thessieu, C. Pfleiderer, A. Stepanov, J. Flouquet, Field dependence of the magnetic quantum phase transition in MnSi. J. Phys., Condens. Matter **9**(31), 6677–6687 (1997)
43. Y.J. Uemura, T. Goko, I.M. Gat-Malureanu, J.P. Carlo, P.L. Russo, A.T. Savici, A. Aczel, G.J. MacDougall, J. Rodoriguez, G.M. Luke, S.R. Dunsiger, A. McCollam, J. Arai, C. Pfleiderer, P. Böni, K. Yoshimura, E. Baggio-Saitovitch, M.B. Fontes, J. Larrea, Y.V. Sushko, J. Sereni, Phase separation and suppression of critical dynamics at quantum transitions of itinerant magnets: MnSi and $(Sr_{1-x}Ca_x)RuO_3$. Nat. Phys. **3**, 34 (2007)
44. T. Westerkamp, M. Deppe, R. Küchler, M. Brando, C. Geibel, P. Gegenwart, A.P. Pikul, F. Steglich, Kondo-cluster-glass state near a ferromagnetic quantum phase transition. Phys. Rev. Lett. **102**(20), 206404 (2009). doi10.1103/PhysRevLett.102.206404
45. M. Yokoyama, H. Amitsuka, K. Tenya, K. Watanabe, S. Kawarazaki, H. Yoshizawa, J.A. Mydosh, Competition between hidden order and antiferromagnetism in URu_2Si_2 under uniaxial stress studied by neutron scattering. Phys. Rev. B **72**, 214419 (2005)